

Bjorken Flow, Plasma Instabilities, and Thermalization

Alexi Kurkela and Guy D. Moore

*Department of Physics, McGill University,
3600 rue University, Montréal QC H3A 2T8, Canada*

(Dated: August 2011)

Abstract

At asymptotically high energies, thermalization in heavy ion collisions can be described via weak-coupling QCD. We present a complete treatment of how thermalization proceeds, at the parametric weak-coupling level. We show that plasma instabilities dominate the dynamics, from immediately after the collision until well after the plasma becomes nearly in equilibrium. Initially they drive the system close to isotropy, but Bjorken expansion and increasing diluteness makes the system again become more anisotropic. At time $\tau \sim \alpha^{-\frac{12}{5}} Q_s^{-1}$ the dynamics become dominated by a nearly-thermal bath; and at time $\tau \sim \alpha^{\frac{5}{2}} Q_s^{-1}$ the bath comes to dominate the energy density, completing thermalization. After this time there is a nearly isotropic and thermal Quark-Gluon Plasma.

I. INTRODUCTION AND SUMMARY

Relativistic heavy ion experiments have given us new insights into the dynamics of hot QCD [1, 2]. One of the most striking results is the success of a hydrodynamic description [3, 4]. This seems to imply that the hot QCD matter generated in a heavy ion collision thermalizes quite quickly and then has a period as a nearly thermal medium well described by hydrodynamics (which is predicated on the assumption of local near-equilibrium). Theoretically, we have no idea why this should be true. In fact, we do not even understand early thermalization in the theoretically clean case where we consider the limit of large nuclei at arbitrarily high energy per nucleon. In this limit, the very early dynamics are believed to be well understood, in the framework of the “colored glass condensate” [5, 6] and its post-collision debris, the “glasma” [7]. According to this description, the initial conditions should be approximately boost-invariant, intense classical colored fields with a single energy scale Q_s , the “saturation scale”. Boost invariance means that the natural coordinates are the transverse directions x, y , rapidity η , and proper time since the collision, τ . We will rename τ to t and generally work in terms of $z \equiv \eta\tau$, the physical distance along the beam direction in η, τ coordinates, which expands (red-shifts) linearly with time (Bjorken expansion). The scale Q_s increases with increasing nuclear size and with increasing energy per nucleon [8], so in principle this scale becomes large in the limit of interest (though whether this is true in practice at achievable energies is another matter). Provided that $Q_s \gg \Lambda_{\text{QCD}}$, physics at the scale Q_s should be characterized by weakly-coupled QCD, with the coupling taking a characteristic value $\alpha_s(Q_s) \ll 1$ (henceforth we write $\alpha_s(Q_s)$ as α). Weak coupling should make the theoretical problem easier to address. Nevertheless, the subsequent evolution of these fields is not well understood.

The most comprehensive attempt to date to describe thermalization at central rapidities from these initial conditions was by Baier, Mueller, Schiff and Son (BMSS) [9]. They argued that the medium made up of $p \sim Q_s$ excitations becomes anisotropic and dilute; but LPM suppressed radiation of lower energy daughters generates a bath of $p \ll Q_s$ excitations which come to dominate the dynamics and lead to the breakup of the $p \sim Q_s$ “hard” “parent” excitations into a thermal bath. However, as pointed out by Arnold, Lenaghan and Moore [10], their discussion ignored the physics of plasma instabilities [11, 12], which should dominate at least the early stages of the dynamics. The role of plasma instabilities in these early stages was considered analytically by Bödeker [13] and by a mix of analytic and numerical considerations by Arnold and Moore [14]. Classical field simulations with plasma instabilities were considered by Romatschke and Venugopalan [15], and several groups made related studies [16]. However, none of these studies followed the dynamics past the early stages or explained how final thermalization occurs.

In this paper we will take advantage of our recent study of the dynamics of weakly coupled gauge theories out of equilibrium (Ref. [17], henceforth “KM1”) to give a purely analytical and parametric description of how “the glasma” should thermalize when Q_s is such a large scale that $\alpha \ll 1$. The initial state of the glasma should be well described by intense classical fields with much longer coherence in the η direction than in the transverse xy plane [7]. That is, the initial conditions are very anisotropic, with a longer coherence length (smaller mean wave number) in the η direction. But we find (as suggested by Ref. [15]) that plasma instabilities rapidly reorganize this into a configuration which is only anisotropic at the $\mathcal{O}(1)$ level.

From this point we find *two* attractor solutions. In one solution, the plasma becomes

highly anisotropic. Bjorken expansion increases the anisotropy but does not lower the wave-number of typical excitations. This leads to a dilute plasma of wave-number $p \sim Q_s$ excitations. This solution is similar to the one found by BMSS [9], except that plasma instabilities dominate the dynamics (as proposed in Ref. [10] and discussed in Refs. [13, 14]). In this solution the momentum space anisotropy grows with time as $t^{\frac{1}{3}}$. In the other attractor solution, the plasma becomes nearly isotropic at a time t longer than Q_s^{-1} by at most logarithms of α . Plasma instabilities resist Bjorken expansion to keep the plasma nearly isotropic. The typical excitation energy falls with time, and the typical occupancy falls but not as fast as in the first solution. This solution is somewhat like the one recently suggested by Blaizot, Gelis, Liao, McLerran, and Venugopalan [18], except that we find that plasma instabilities play a key role in the dynamics and that no Bose-Einstein condensate forms. Fully nonperturbative and nonequilibrium early-time dynamics determine which attractor the system finds. But we argue that the path from the initial conditions to the more anisotropic attractor is much more likely.

Assuming the first (strongly anisotropic) attractor is correct, we find that a nearly-thermal bath of low-momentum ($p \sim T \ll Q_s$) excitations forms and comes to dominate the dynamics at time $t \sim \alpha^{\frac{-12}{5}} Q_s^{-1}$. By $t \sim \alpha^{\frac{-5}{2}} Q_s^{-1}$ the soft bath causes the “hard” $p \sim Q_s$ excitations to disintegrate and the system becomes nearly isotropic and thermal, with a temperature $T_{\text{final}} \sim \alpha^{\frac{-11}{24}} Q_s^{\frac{2}{3}} t^{\frac{-1}{3}}$. But while nearly thermal, the system is initially non-Newtonian; anomalous viscosity [19] (due to plasma instabilities) controls the level of isotropy until $t \sim \alpha^{\frac{-45}{16}} Q_s^{-1}$, after which the fluid becomes Newtonian. Before $t \sim \alpha^{\frac{-5}{2}} Q_s^{-1}$ the plasma is far from equilibrium; we parametrically estimate the (quite complicated) phase space particle number density at all momenta $p \leq Q_s$ and all times from Q_s^{-1} to final thermalization. The results are presented in Figure 5 and Table II.

Our results indicate a faster breakup of the hard $p \sim Q_s$ excitations than the old estimate $t \sim \alpha^{\frac{-13}{5}} Q_s^{-1}$ from BMSS [9], but still somewhat slower than the absolute lower bound of $\alpha^{\frac{-7}{3}} Q_s^{-1}$ derived by Arnold and Lenaghan [20]. But it is consistent with the estimate for full thermalization times presented in KM1, who claim $t_{\text{eq}} \sim \alpha^{\frac{-13}{7}} Q_s^{\frac{5}{7}} T^{\frac{-12}{7}}$; inserting T_{final} returns $t \sim \alpha^{\frac{-5}{2}} Q_s^{-1}$.

II. INITIAL CONDITIONS AND ATTRACTORS

As we briefly mentioned in the introduction, an extensive literature on the small- x behavior of large nuclei (see Ref. [8]) and small- x evolution in heavy ion collisions [5, 7] indicates that, at time $t \sim Q_s$, the debris of a heavy ion collision is dominated by classical gluon fields with coherence length $l \sim 1/Q_s$ in the xy plane, much longer coherence in $z = \eta t$, and energy density $\varepsilon(t \sim Q_s^{-1}) \sim \alpha^{-1} Q_s^4$. At times $t > Q_s^{-1}$ these fields have lost phase coherence and the evolution should be described with the tools we introduced in KM1, modified to include the Bjorken expansion of the geometry.

A. Combining KM1 with Bjorken expansion

We begin by introducing notation, including the notation used in KM1. In KM1 we considered the evolution of a system with a single dominant characteristic wave number Q in a time-independent geometry. The system is characterized by a scale Q (which need

Variable	Describes	Detailed Definition
a	time	$t = \alpha^{-a} Q_s^{-1}$
b	Typical momentum	$Q \sim \alpha^b Q_s$, where $f(p \gg Q) \ll f(p \sim Q)$
c	Mean occupancy	$f(\mathbf{p} = Q\hat{x}) \sim \alpha^{-c}$
d	Anisotropy	$d < 0$: $f(Q\hat{x}) - f(Q\hat{z}) \sim \alpha^{-d} f(Q)$ $d > 0$: $f(p_z, \mathbf{p}_\perp) \ll f(0, \mathbf{p}_\perp)$ if $p_z > \alpha^d \mathbf{p}_\perp $

TABLE I: Brief summary of our log notation for the most important descriptors of the system

not be Q_s ; we will write $Q = \alpha^b Q_s$, a typical occupancy $f(p \sim Q) \sim \alpha^{-c}$, and a degree of anisotropy characterized by d . For $d > 0$ most excitations have $p_z \lesssim \alpha^d p$ and we write $\delta \equiv \alpha^d$. The occupancy $f(p) \sim \alpha^{-c}$ applies for $p_z < \delta p$, outside this range the occupancy is small, so the particle number and energy densities are

$$\text{for } d > 0, \quad n \sim \alpha^{d-c} Q^3 \quad \text{and} \quad \varepsilon \sim \alpha^{d-c} Q^4 \sim \alpha^{d-c+4b} Q_s^4. \quad (2.1)$$

For $d < 0$ the particle number is nearly direction independent, but the direction dependence varies with relative amplitude $\epsilon \equiv \alpha^{-d}$ – that is, $(f(Q\hat{x}) - f(Q\hat{z}))/f(Q) \sim \epsilon$. Therefore, for $d < 0$, the particle number and energy densities are

$$\text{for } d < 0, \quad n \sim \alpha^{-c} Q^3 \quad \text{and} \quad \varepsilon \sim \alpha^{-c} Q^4 \sim \alpha^{-c+4b} Q_s^4. \quad (2.2)$$

We will also introduce one more logarithmic variable; we will write the time as $t = \alpha^{-a} Q_s^{-1}$ (or $a \equiv \ln(tQ_s)/\ln(1/\alpha)$). The initial conditions are fixed at $t \sim Q_s^{-1}$, which is $a = 0$. Parametrically later times are $a > 0$. Our notations are summarized in Table I.

According to KM1, the occupancy–anisotropy or c, d plane is divided into four regions, shown in Figure 1. At large anisotropy the dynamics are dominated by magnetic or “Weibel” [21] plasma instabilities. That means that certain long-wavelength magnetic fields grow to large amplitudes; there are associated electric fields but they are much weaker. Magnetic fields change an excitation’s direction without changing the energy; so the main physics in this region involves the randomization of excitations’ directions. Induced (bremsstrahlung) emission or merging of excitations also occurs but is subdominant. For less isotropic but over-occupied systems ($1 > c > 0$ and $d < (c - 1)/3$), ordinary scattering dominates the dynamics. Elastic scattering drives the system towards isotropy, and inelastic scattering drives the mean occupancy c towards zero. The two types of scattering are of comparable efficiency (in stark contrast to scalar field theory). For underoccupied systems below some level of anisotropy, the main physics is that a bath of smaller-momentum excitations forms and eventually causes the dominant excitations to shower and join this bath. The last region, of extremely high occupancies, exhibits Nielsen-Olesen instabilities [22]. This region has no relevance for us. The arrows in Figure 1 show qualitatively how these dynamics cause c, d to evolve with time.

All this is for a homogeneous and non-expanding system. But the debris of a heavy ion collision expand. In our choice of coordinates the system is nearly statistically homogeneous, but the z direction grows linearly with time. This Bjorken expansion red-shifts away the z component of momentum, increasing the anisotropy of the system, and raising d . And for $d < 0$ it lowers the typical excitation’s energy, increasing b . In the scattering, plasma unstable, and Nielsen-Olesen regions the evolution of b, c, d will be determined by an interplay of the equilibration processes and Bjorken expansion.

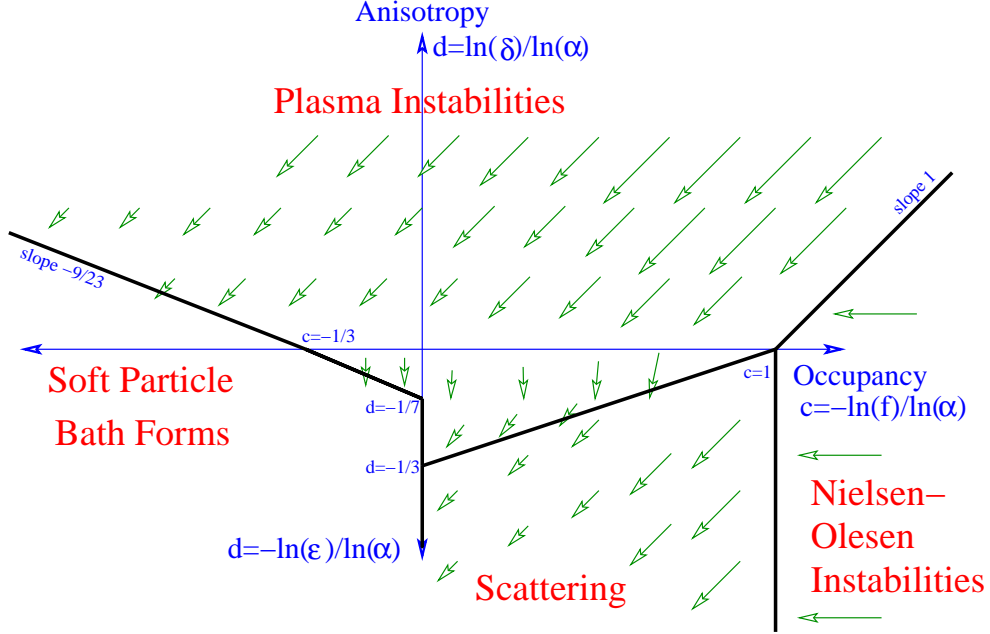


FIG. 1: Simplified version of Figure 1 from KM1 [17]. The vertical axis represents how anisotropic the dominant excitations are; the horizontal axis shows how large the dominant excitation occupancies are. The labels indicate what the dominant physics is in each region; the arrows suggest how those dynamics “move” the system in this two-dimensional space. There are no arrows in the “soft particle bath” region because here the typical excitations break up and are replaced by something very different.

B. Initial conditions and attractors

The initial conditions we described above have $d > 0$ and $c = 1 + d$ at time $t \sim Q_s^{-1}$. This is the point marked “Initial Condition” in Figure 2. The figure also shows two attractor solutions which we find, which we now explain in more detail. By an attractor we mean a path on the c, d plane, such that a system relatively close to the path will fall onto and then follow the path as a result of the combination of dynamics and Bjorken expansion. There are two attractors because there is a fundamental difference between the dynamics of a system with large anisotropy versus a system with small anisotropy. This difference turns out to allow solutions of either type.

Consider first a system which is highly anisotropic, so the typical excitation has $p_z \ll |\mathbf{p}|$. Then Bjorken expansion does not change the typical excitation’s energy. And angle randomization – such as that induced by plasma instabilities – increases the region of phase space which is occupied, and therefore brings down the typical occupancy (reduces c). But consider instead a system which is only weakly anisotropic. Typical excitations have $|p_z| \sim |\mathbf{p}|$, and therefore Bjorken expansion reduces typical excitation energy. And since angle randomization is mixing modes of nearly the same occupancy, it has little impact on the typical occupancy. These fundamental differences mean that we have to treat the two cases, $d > 0$ and $d < 0$, separately. And we will find an attractor in each. Specifically, we will find for $d > 0$,

$$d = \frac{a}{8}, \quad c = 1 - \frac{7a}{8}, \quad b = 0, \quad (\text{attractor 1}) \quad (2.3)$$

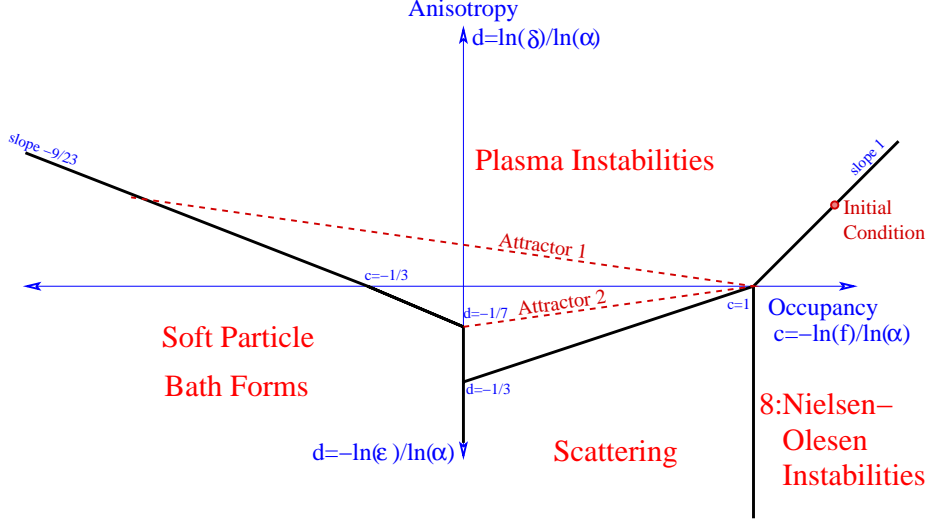


FIG. 2: Occupancy-anisotropy plane, the initial conditions from heavy ion collisions, and the two attractor solutions we find.

while for $d < 0$ there is another attractive solution,

$$d = -\frac{8a}{135}, \quad c = 1 - \frac{56a}{135}, \quad b = \frac{31a}{135}. \quad (\text{attractor 2}) \quad (2.4)$$

These attractors, and the initial conditions, are displayed in Figure 2.

C. First (anisotropic) attractor

First consider the case $d > 0$, where most excitations have $p_z \ll |\mathbf{p}|$. This region lies entirely in the plasma instabilities dominated region in Figure 1 provided $c > -1/3$ (as it initially is). To describe evolution in this region it is convenient to think of the descriptors of a system, b , c , and d , as functions of time or of a , and to ask about their a derivatives; $c' \equiv dc(a)/da$ and similarly for b' , d' . Each quantity evolves due to Bjorken expansion and due to the effects of dynamics, principally plasma instabilities; we will write $c' = c'|_{\text{Bjorken}} + c'|_{\text{dyn}}$ to distinguish the part of the evolution from each effect.

The effect of Bjorken expansion is a red-shifting of the p_z component of momentum,

$$\frac{dp_z}{dt} = -\frac{p_z}{t} \quad (\text{Bjorken expansion}). \quad (2.5)$$

This does not change c ; occupied states retain their occupancy, they just change the value of momentum. It also does not change b ; since $p_z \ll |\mathbf{p}|$, the typical excitation's energy is not changed. Thus, $c'|_{\text{Bjorken}} = 0 = b'|_{\text{Bjorken}}$. But Bjorken expansion does lead to an increase in d . Recall that $\delta \equiv (p_z/p)_{\text{RMS}} = \alpha^d$. The angle δ evolves according to

$$\frac{d\delta}{dt} = \frac{d\delta}{dp_z} \frac{dp_z}{dt} = \frac{\delta}{p_z} \frac{dp_z}{dt} = -\frac{\delta}{t}, \quad (2.6)$$

which using Eq. (2.5) and the definitions of a , d becomes

$$d'|_{\text{Bjorken}} = \frac{d(d)}{da} = \frac{d(d)}{dt} \frac{dt}{da} = \frac{d(\ln(\delta)/\ln(\alpha))}{dt} \frac{dt}{d(\ln(tQ_s)/\ln(\alpha^{-1}))} = -\frac{td\delta}{\delta dt} = +1. \quad (2.7)$$

Now we need to add the effect of plasma instabilities. As mentioned, the dominant thing the instabilities do is to deflect excitations, widening their angular range. This changes c and d , but not the typical energy b ; $b'|_{\text{dyn}} = 0$. Since $b'|_{\text{Bjorken}} = 0$ as well, we find $b' = 0$ and therefore $b = 0$; the typical excitation energy remains $Q = Q_s$. Dynamics also cannot change the total energy density ε . According to Eq. (2.1), ε depends on the combination $d - c + 4b$. Since $b' = 0$, we learn that $d'|_{\text{dyn}} - c'|_{\text{dyn}} = 0$. Combining with Eq. (2.7), we learn that $d' - c' = 1$. Since initially $c - d = 1$, we have

$$b = 0, \quad c - d = 1 - a \quad (d > 0 \text{ case}). \quad (2.8)$$

Therefore the state of the system at a given time t (or a given value of a) is determined by $d(a)$; c is fixed to be $c = 1 + d - a$.

To finish determining the dynamics we need to find out how fast plasma instabilities cause the level of anisotropy to change. According to KM1, there is a time scale t_{broaden} which determines how long it takes the plasma instabilities to significantly increase the range of angles of $p \sim Q$ excitations (to reduce d). The anisotropy therefore evolves at

$$\frac{d(d)}{dt} \sim -\frac{1}{t_{\text{broaden}}} \quad \Rightarrow \quad d'|_{\text{dyn}} = \frac{-t}{t_{\text{broaden}}} = -\alpha^{-a} Q_s^{-1} t_{\text{broaden}}^{-1}. \quad (2.9)$$

According to KM1 [17], the time scale t_{broaden} is

$$t_{\text{broaden}} \sim \begin{cases} \alpha^{\frac{c-d-1}{2}} Q^{-1} & d > \frac{1-c}{3}, \\ \alpha^{\frac{3c+5d-3}{2}} Q^{-1} & d < \frac{1-c}{3}. \end{cases} \quad (2.10)$$

Combining with Eq. (2.8) and Eq. (2.9), we find

$$d'|_{\text{dyn}} \sim \begin{cases} -\alpha^{\frac{-a}{2}} & d > \frac{1-c}{3}, \\ -\alpha^{\frac{a-8d}{2}} & d < \frac{1-c}{3}. \end{cases} \quad (2.11)$$

At a time a during the evolution, d might take its value on, above, or below the attractor. Since we have two constraints, Eq. (2.8), on b, c, d , the possible deviation from the attractor is completely fixed by the value $d(a)$. If $d(a) > a/8$ then $d'|_{\text{dyn}} \ll -1$ and d falls very rapidly, on a time scale shorter than the age of the system. If $d < a/8$ then $d'|_{\text{dyn}} \simeq 0$ and $d' = 1$. In this case d grows linearly with a , rapidly exceeding $a/8$. Therefore the solution $d = a/8$ is an attractor. The rest of Eq. (2.3) follows from Eq. (2.8). According to Figure 2, this solution makes sense until it reaches the point $d = 3/10$, $c = -11/10$, which occurs at $a = 12/5$ ($t \sim \alpha^{\frac{-12}{5}} Q_s^{-1}$). After this time a soft bath forms and takes over the dynamics. We will return to these ‘‘late-time’’ dynamics in the next section.

D. Second attractor

Now consider the case $d < 0$, that is, systems which are nearly isotropic. Now Eq. (2.5) is still correct, but since $\langle p_z^2 \rangle \simeq \mathbf{p}^2/3$, expansion now changes the typical particle energy,

$$b'|_{\text{Bjorken}} = 1/3. \quad (2.12)$$

Correspondingly, the energy density falls with time as $\varepsilon \sim t^{-4/3}$ (t^{-1} due to dilution and $t^{-1/3}$ due to the work done by longitudinal pressure). Then Eq. (2.2) becomes (compare with Eq. (2.8))

$$-c' + 4b' = 4/3 \quad \text{or} \quad 4b = c - 1 + 4a/3. \quad (2.13)$$

We can use this expression to eliminate b in favor of c, d in what follows.

Next we find the effect of expansion on d . A reduction of p_z by $p_z \rightarrow p_z(1 - \epsilon)$ would induce an anisotropy of ϵ . Since $d \equiv \ln(\epsilon)/\ln(1/\alpha)$, d is very sensitive to expansion:

$$d'|_{\text{Bjorken}} \sim \epsilon^{-1} = \alpha^d \gg 1. \quad (2.14)$$

In any self-consistent solution, $d'|_{\text{dyn}}$ will have to be compensatingly large, so $d' = (d'|_{\text{Bjorken}} + d'|_{\text{dyn}}) \lesssim 1$.

We can immediately rule out the existence of an attractor solution in the scattering region, $d < (-1 + c)/3$. In this region, number-changing processes are as efficient as direction-changing elastic processes.¹ Therefore $c'|_{\text{dyn}} \sim d'|_{\text{dyn}}$.² So in the scattering region, either $d'|_{\text{dyn}} \sim 1$, in which case d rises very fast due to $d'|_{\text{Bjorken}} \gg 1$, or $d'|_{\text{dyn}} \gg 1$, in which case $c'|_{\text{dyn}} \gg 1$ and the system evolves very fast to lower occupancy. Since lower occupancy features slower dynamics, both $c'|_{\text{dyn}}$ and $d'|_{\text{dyn}}$ would then collapse, again allowing d to rise into the plasma-unstable region.

So consider the region with important plasma instabilities, $0 > d > (-1 + c)/3$. According to KM1, there are two relevant time scales here: t_{broaden} , the time scale for plasma instabilities to cause large-angle direction change; and t_{merge} , the time scale for plasma-instability induced number-changing processes. (Think of these as hard synchrotron radiation, induced as the excitations bend in the magnetic fields; but for over-occupied systems the synchrotron absorption process is more important than emission.) The time scales are (also using Eq. (2.13))

$$0 > d > \frac{c-1}{3} : \quad \begin{aligned} t_{\text{broaden}} &\sim \alpha^{\frac{3d-3+3c}{2}} Q^{-1} \sim \alpha^{\frac{3d-3+3c-2b+2a}{2}} t \sim \alpha^{\frac{18d+15(c-1)+8a}{12}} t, \\ t_{\text{merge}} &\sim \alpha^{\frac{3d-7+7c}{4}} Q^{-1} \sim \alpha^{\frac{3d-7+7c-4b+4a}{4}} t \sim \alpha^{\frac{9d+18(c-1)+8a}{12}} t. \end{aligned} \quad (2.15)$$

Merging (two particles joining into one with the sum of the initial particles' energy) raises the typical particle energy and lowers the occupancy. So

$$0 > d > \frac{c-1}{3} : \quad c'|_{\text{dyn}} \sim -\frac{t}{t_{\text{merge}}}. \quad (2.16)$$

¹ Since there is some confusion in the literature on this point [18], we will summarize why this is true. The rate for an excitation to undergo a generic-angle $2 \leftrightarrow 2$ process is $\alpha^{2-2c} Q^{-1}$ (α^2 for the two vertices, α^{-2c} for two Bose factors). Small-angle scattering is enhanced by a factor $Q^2/m^2 \sim \alpha^{-1+c}$ because of the Coulomb divergence; but a small angle scattering does little to drive the system towards equilibrium. Adding a hard radiation or merging onto a small-angle scattering process reduces the rate by a factor of α^{1-c} (α for the vertex, α^{-c} for a Bose stimulation factor for the new external state; phase space factors are canceled by collinear factors as usual in ISR or FSR), yielding a rate of $\alpha^{2-2c} Q^{-1}$. If $f(p \ll Q) \propto p^{-1}$ then the rate in the infrared is actually larger by a factor of Q/p , which makes the development of a negative chemical potential impossible (contrary to the assumptions of [18]). This point is discussed at some length in Ref. [23], section III E.

² The only exception is if $c = 0$, so number changing processes are in equilibrium. That is, there can be nearly-thermal, scattering dominated systems, just not ones with parametrically large occupancy.

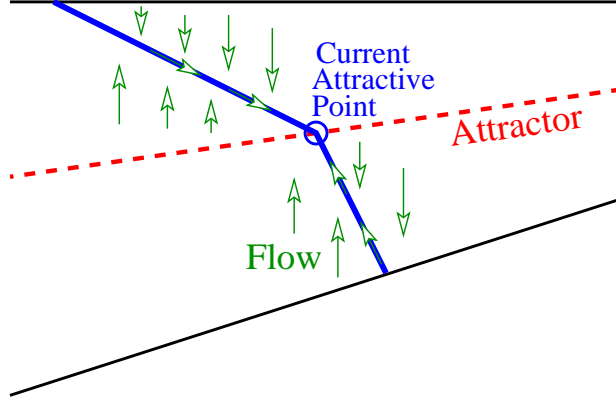


FIG. 3: Evolution near the second attractor. At a given time a , one point on the attractor line (circled in blue) is preferred. Above the solid blue line, the dynamics rapidly lowers the anisotropy; above the line, Bjorken expansion rapidly raises it (as suggested by green arrows). On the blue line, number-changing processes move the system towards the blue circled point.

Broadening leads towards isotropy, lowering d . But so does merging; as discussed in KM1, when merging is induced by plasma instabilities, the particles near the xy plane merge more often than those with large p_z , reducing the number of in-plane excitations. This last effect is independent of the anisotropy ϵ , while angle randomization only affects the $\mathcal{O}(\epsilon)$ angle-anisotropic part of the distribution. Therefore [17]

$$d'|_{\text{dyn}} = - \left(\frac{t}{t_{\text{broaden}}} + \alpha^d \frac{t}{t_{\text{merge}}} \right). \quad (2.17)$$

The t_{broaden} term dominates if $0 > d > (-1 + c)/7$; for $d < (-1 + c)/7$ the t_{merge} term dominates.

Now we show that Eq. (2.4) constitutes an attractor. While in the $d > 0$ case we had two constraints on b, c, d , now we have only one constraint, Eq. (2.13). So if we are off the attractor at time a , we are at some point in the c, d plane. Figure 3 shows how c, d might deviate from the attractor solution, Eq. (2.4), at some given time a . The blue line is the line where $-d'|_{\text{dyn}} = d'|_{\text{Bjorken}}$: using Eq. (2.14), Eq. (2.17) and Eq. (2.15),

$$-d'|_{\text{dyn}} = d'|_{\text{Bjorken}} \quad \text{if} \quad \begin{cases} d = \frac{1-c}{2} - \frac{4a}{15}, & d > \frac{c-1}{7}, \\ d = 2(1-c) - \frac{8a}{9} & d < \frac{c-1}{7}. \end{cases} \quad (2.18)$$

Above this line, $|d'|_{\text{dyn}}| > d'|_{\text{Bjorken}}$. Since both are large, d' is large and negative here. Below the line, $|d'|_{\text{dyn}}| < d'|_{\text{Bjorken}}$ and d' is large and positive. In either case the dynamics drive d to the line on a time scale short compared to the system's age.

Next we must check the evolution of c on the blue line in Figure 3, to see whether it is driven towards the attractor. To the left of the line, where $d > d_{\text{attract}}$ and $c < c_{\text{attract}}$, Eq. (2.15), Eq. (2.16), and Eq. (2.18) show that $c' \simeq 0$. Since the attractor moves towards lower c with time (Eq. (2.4)), points here move towards being on the attractor. To the right of the line, where $c > c_{\text{attract}}$, Eq. (2.16) and Eq. (2.17) show that $c'|_{\text{dyn}} \sim \alpha^d d'|_{\text{dyn}} \sim -1$. In fact it is more negative than -1, since every merging process changes typical occupancy, but only the anisotropic part of merging processes change anisotropy. Therefore c would fall quickly when it is greater than the attractor value. This verifies that the solution, Eq. (2.4), constitutes an attractor.

Of course, it might somehow occur that the amplitude of plasma instabilities overshoots the level where nonlinear interactions normally limit instability growth. That would allow the unstable fields to grow larger, and angle change to be faster, than the estimates given above (which are based on steady-state plasma instability evolution [17]). For instance, it is known that, if the system is very anisotropic and if instabilities start with extremely small initial amplitudes, this can occur [25, 26]. But we claim that even such an “overshoot” cannot lead to near-isotropy.

First, note that the plasma-unstable fields have much larger magnetic than electric field amplitude. Therefore, they deflect hard excitations more efficiently and they absorb their energy. The time scale for large-angle deflection is shorter than the time scale for large energy absorption; so the plasma-unstable fields never dominate the energy density, which remains in the hard excitations. So the only way to get isotropy is to get large-angle deflection.

We showed above that the scales m and Q_s become separated; $m \ll Q_s$ (at least by $\log(1/\alpha)$). The unstable fields have wave numbers $k \sim m$. For a field of wave number $k \sim m \ll Q_s$ to bend excitations of momentum Q_s by an order-1 angle in a time scale $1/m$, the force would have to be $dp/dt \sim mQ_s$, requiring a magnetic field of strength $B \sim mQ_s/g$. But in nonabelian field theory, whenever a magnetic field of wave number k exceeds the field strength $B \geq k^2/g$, it becomes Nielsen-Olesen unstable [22], leading to the very rapid ($t \lesssim 1/k = 1/m$) collapse of any such magnetic field. Therefore the magnetic fields associated with plasma instabilities can never grow larger than $B \sim m^2/g$ – too small to deflect hard $p \sim Q_s$ excitations by large angles.

In the remainder of the paper we will concentrate on filling in all details about the development of the system, assuming it follows the first attractor.

III. DETAILED EVOLUTION ALONG THE FIRST ATTRACTOR

In the previous Section, we described how the occupancies c and the anisotropy parameter d of the primary particles with $p \sim Q_s$ evolve with time along the attractor 1, until at the time $a = 12/5$, when the momentum diffusion experienced by the primary particles is taken over by the soft sector. In this Section we describe the details how the soft sector evolves during this time, and we describe in detail what happens after the soft sector takes over the dynamics. In particular, we find the occupancies and angular ranges of all excitations throughout the evolution of the system. The results of this Section are collected in Figure 5 and Table II.

We divide the evolution in three main stages. In the early stage the primary particles have occupancies larger than 1, and all processes involving these modes are stimulated. During this stage, the system grows steadily more anisotropic and radiated daughters become less and less important. Incidentally, this means that classical Yang-Mills theory under Bjorken expansion never isotropizes and the interactions become weaker with time.

At the time $a = 8/7$, the attractor 1 crosses the c -axis in Figure 2, and the occupancies of the hard excitations become small. Therefore, the Bose stimulation of processes involving hard excitations is lost. This is the middle stage. The loss of stimulation makes the interaction rates decrease *more slowly*, and the soft sector will start to affect the dynamics. The soft sector is also anisotropic and therefore has its own unstable modes. During the

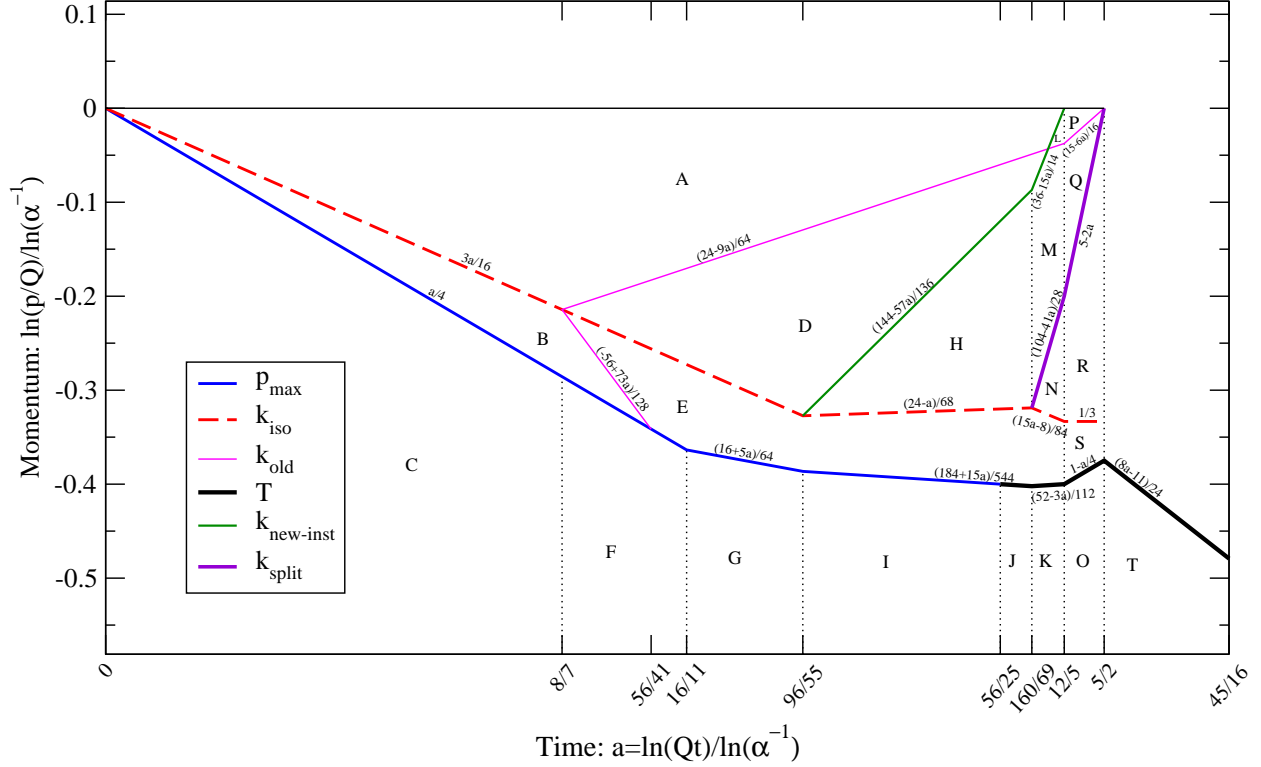


FIG. 5: Log-log plot of the time-momentum plane, divided into regions with distinct behaviors for the angular range of excitations about the xy plane, θ , and the occupancy $f(p)$. The horizontal axis is a defined as $t = \alpha^{-a} Q_s^{-1}$ or $a = -\ln(tQ_s)/\ln(\alpha)$. The vertical axis is the log of momentum. The equations describing lines are written in shorthand, so for instance $(8 - 3a)/16$ means $p = Q_s \alpha^{(8-3a)/16}$. The letters A – T refer to Table II.

second stage, the momentum diffusion⁴ $\hat{q} \equiv dp_{\perp}^2/dt$ arising from these new plasma instabilities increases relative to the “primary” instabilities of the hard particles. The new plasma instabilities come to dominate \hat{q} at large angles at the time $a = 96/55$. But \hat{q} at narrow angles, experienced by the primary excitations, remains dominated by the “primary” instabilities. Most of the particle number in the soft sector is in a nearly isotropic bath, whose distribution forms an $f(p) \propto 1/p$ “tail” below a cutoff scale p_{\max} . Initially $f(p_{\max}) \gg 1$, but at the time $a = 56/25$, $f(p_{\max}) = 1$ and the soft bath becomes nearly thermal.

Plasma instabilities from the nearly-thermal bath grow to dominate at all angles at time $a = 12/5$, which is where attractor 1 in Figure 2 intersects with the boundary between the regions labeled “Plasma Instabilities” and “Soft Particle Bath Forms”. Thereafter, the broadening of the hard primary particles will be controlled by the soft sector and its plasma instabilities. The instabilities cause hard particles to undergo successive splitting processes, depositing their energy into the thermal bath, increasing its temperature. At time $a = 5/2$, the primary $p \sim Q_s$ particles have had time to break up completely, leaving only a nearly isotropic thermal bath. We now discuss these stages in more detail.

⁴ Here and in the following, “transverse” or p_{\perp} refers to the directions transverse to the initial momentum of the particle, not the directions transverse to the beam axis.

Region	θ range	Occupancy $f(p)$	Region	θ range	Occupancy $f(p)$
A	$\alpha^{\frac{a}{8}}(Q_s/p)^{\frac{2}{3}}$	$\alpha^{\frac{-8+7a}{8}}(Q_s/p)^{\frac{1}{6}}$	K	1	$\alpha^{\frac{52-3a}{112}}(Q_s/p)^1$
B	1	$\alpha^{\frac{-14+27a}{14}}(Q_s/p)^{\frac{81}{14}}$	L	$\alpha^{\frac{48-13a}{56}}(Q_s/p)^1$	$\alpha^{\frac{-104+69a}{56}}(Q_s/p)^{\frac{-1}{6}}$
C	1	$\alpha^{\frac{-8+7a}{8}}(Q_s/p)^1$	M	$\alpha^{\frac{48-13a}{56}}(Q_s/p)^1$	$\alpha^{\frac{-6+6a}{7}}(Q_s/p)^{\frac{5}{2}}$
D	$\alpha^{\frac{a}{8}}(Q_s/p)^{\frac{2}{3}}$	$\alpha^{\frac{a}{2}}(Q_s/p)^{\frac{17}{6}}$	N	$\alpha^{\frac{-8+15a}{112}}(Q_s/p)^{\frac{3}{4}}$	$\alpha^{\frac{8+55a}{112}}(Q_s/p)^{\frac{11}{4}}$
E	1	$\alpha^{\frac{5a}{8}}(Q_s/p)^{\frac{7}{2}}$	O	1	$\alpha^{\frac{4-a}{4}}(Q_s/p)^1$
F	1	$(Q_s/p)^1$	P	$\alpha^{\frac{3-a}{2}}(Q_s/p)^1$	$\alpha^{\frac{-5+3a}{2}}(Q_s/p)^{\frac{-1}{6}}$
G	1	$\alpha^{\frac{-80+55a}{128}}(Q_s/p)^1$	Q	$\alpha^{\frac{3-a}{2}}(Q_s/p)^1$	$\alpha^{\frac{a}{2}}(Q_s/p)^{\frac{5}{2}}$
H	$\alpha^{\frac{24-a}{68}}(Q_s/p)^1$	$\alpha^{\frac{-48+87a}{136}}(Q_s/p)^{\frac{5}{2}}$	R	$\alpha^{\frac{1}{4}}(Q_s/p)^{\frac{3}{4}}$	$\alpha^{\frac{5}{4}}(Q_s/p)^{\frac{11}{4}}$
I	1	$\alpha^{\frac{-920+605a}{1088}}(Q_s/p)^1$	S	1	$\alpha^{\frac{3}{2}}(Q_s/p)^{\frac{7}{2}}$
J	1	$\alpha^{\frac{184+15a}{544}}(Q_s/p)^1$	T	1	$\alpha^{\frac{8a-11}{24}}(Q_s/p)^1$

TABLE II: Angular range of excitations and typical occupancies for the regions labeled in Figure 5.

A. Early stage: $a < 8/7$

1. Angular distribution, the scale k_{iso}

We will now find the angular ranges and occupancies of the soft sector during the evolution. Plasma instabilities give rise to angle dependent transverse momentum diffusion characterized by \hat{q} of size [17]

$$\hat{q} \sim \begin{cases} \delta^{-2}m^3 \sim \alpha^{\frac{5a}{4}}Q_s^3, & p_z \lesssim \delta p_\perp, p > \delta^{-2}m \sim \alpha^{\frac{a}{4}}Q_s, \\ \delta^{-1}\theta^{-1}m^3 \sim \theta^{-1}\alpha^{\frac{11a}{8}}Q_s^3, & p_z/p_\perp \equiv \theta, p > m/(\delta\theta), \end{cases} \quad (3.1)$$

where m is the thermal mass

$$m^2 \sim \alpha \int \frac{d^3p}{p} f(p) \sim \alpha^{1-c+d}Q_s^2 \sim \alpha^a Q_s^2, \quad m \sim \alpha^{a/2}Q_s. \quad (3.2)$$

The angular range which excitations of momentum p occupy will be given by

$$\theta^2 p^2 \sim \hat{q}(\theta)t \sim \alpha^{\frac{11a}{8}}\theta^{-1}\alpha^{-a}Q_s^2 \quad \Rightarrow \quad \theta \sim \alpha^{\frac{a}{8}}(Q_s/p)^{\frac{2}{3}}. \quad (3.3)$$

We define the scale where $\theta \sim 1$ as k_{iso} :

$$1 \sim \alpha^{\frac{a}{8}}(Q_s/k_{\text{iso}})^{\frac{2}{3}} \quad \Rightarrow \quad k_{\text{iso}} \sim \alpha^{\frac{3a}{16}}Q_s. \quad (3.4)$$

Below this scale particles are nearly isotropic.

2. Particle production

The instabilities not only change the angular range the soft particles populate; they also affect their occupancies through instability induced splitting processes. Provided $p \geq \delta^{-2}m \sim \alpha^{\frac{a}{4}}Q_s$, particle emission is LPM suppressed. The formation time for an emission is

$$t_{\text{form}}^{-2}(p, \theta) \sim \hat{q}(\theta)p^{-1} \sim \alpha^{\frac{5a}{4}}Q_s^3p^{-1}(\delta/\theta) \quad (3.5)$$

but for our case, in a time t_{form} the radiated daughter only accumulates a transverse momentum of $\sqrt{\hat{q}t_{\text{form}}} < \delta p$, so $\theta \sim \delta$. Ignoring stimulation, the rate each hard particle splits off daughters of momentum p is $d\Gamma/d\ln(p) \equiv \Gamma_{\text{split}} \sim \alpha t_{\text{form}}^{-1}$. Summing over the number density hard particles n_{hard} and including the final-state hard particle stimulation factor $[1+f(Q_s)] \sim \alpha^{-c}$, the number of daughters radiated per logarithmic momentum range in time $t \sim \alpha^{-a}Q_s^{-1}$ is

$$n_{\text{daughter}}(p, a) \sim n_{\text{hard}}\alpha^{-c}\alpha t_{\text{form}}^{-1}t \sim \alpha^{d-c}Q_s^3\alpha^{1-c}\alpha^{\frac{5a}{8}}\alpha^{-a}(Q_s/p)^{\frac{1}{2}} \sim \alpha^{-1+\frac{3a}{2}}Q_s^{\frac{7}{2}}p^{-\frac{1}{2}}. \quad (3.6)$$

3. Redshifting and old particles

As a consequence of expansion, the rate of particle production falls quickly ($\propto \alpha^{\frac{3}{2}a}$), and therefore the distribution of soft particles at a given time a need not to be dominated by the particles emitted during that time scale. The daughters radiated at an earlier time a' are still around, though they have reduced in number and energy due to Bjorken expansion.

For $p > k_{\text{iso}}$, the longitudinal momentum component is parametrically small compared to the total momentum, and the effect of the expansion is simply to reduce the number of particles by a factor $\alpha^{a-a'}$. So the number density of particles, emitted at time a' , which are present at time $a > a'$ is

$$n_{\text{redshift}}(p > k_{\text{iso}}, a; a') \sim \alpha^{a-a'}n_{\text{daughter}}(p, a'). \quad (3.7)$$

For $p < k_{\text{iso}}$, the expansion also decreases the z -component of momentum. The plasma instabilities keep the soft distribution below k_{iso} isotropic so that the net effect of the expansion and angle randomization is to redshift the isotropic spectrum below k_{iso} to smaller momenta, much like in the case of attractor 2;

$$n_{\text{redshift}}(p < k_{\text{iso}}, a; a') \sim \alpha^{a-a'}n_{\text{daughter}}(\alpha^{-\frac{1}{3}(a-a')}p, a'). \quad (3.8)$$

Both above and below k_{iso} , the particle number density at momentum scale p is dominated by particles which were emitted at the scale k_{iso} . For $p > k_{\text{iso}}$, the dominant contribution to $n(p)$ arises from time a' when k_{iso} was p , namely $\alpha^{a'} \sim (p/Q_s)^{\frac{16}{3}}$, so that the particle number density above k_{iso} is

$$n(p) \sim \alpha^{a-a'}\alpha^{-1+\frac{3}{2}a'}Q_s^{\frac{7}{2}}p^{-\frac{1}{2}} \sim \alpha^{-1+a}(p/Q_s)^{\frac{13}{6}}Q_s^3, \quad (3.9)$$

and the corresponding occupancies in the occupied angle region are

$$f(p) \sim \frac{n(p)}{\theta(p)p^3} \sim \alpha^{-1+\frac{7}{8}a}(Q_s/p)^{\frac{1}{6}}. \quad (3.10)$$

This is Region A in Figure 5.

For $p < k_{\text{iso}}$, the particles created at the scale k_{iso} at time a' have just redshifted to scale p at time a provided that

$$\alpha^{\frac{1}{3}(a-a')}k_{\text{iso}}(a') \sim p, \quad (3.11)$$

so that the particle number density at time a is dominated by particles created at the time

$$\alpha^{a'} \sim \alpha^{\frac{16}{7}a}(Q_s/p)^{\frac{48}{7}}. \quad (3.12)$$

The particle number density and occupancies then read

$$n(p) \sim \alpha^{a-a'} \alpha^{-1+\frac{3}{2}a'} Q_s^{\frac{7}{2}} (\alpha^{-\frac{1}{3}(a-a')} p)^{-\frac{1}{2}} \sim \alpha^{-1+\frac{27}{14}a} (Q_s/p)^{\frac{39}{14}} Q_s^3, \quad (3.13)$$

$$f(p) \sim \frac{n(p)}{p^3} \sim \alpha^{-1+\frac{27}{14}a} (Q_s/p)^{\frac{81}{14}}. \quad (3.14)$$

This is Region B in Figure 5.

4. Saturation, the scale p_{\max}

As seen in KM1, distributions that have infrared tails steeper than that of a thermal distribution rearrange themselves very effectively to form a thermal-like tail so that

$$f(p) \propto 1/p, \quad \text{for } p < p_{\max}. \quad (3.15)$$

In particular, if the occupancies of daughters $f(p)$ exceed

$$f(p) \sim \frac{Q_s}{p} [1+f(Q_s)], \quad (3.16)$$

the rate for the daughter particles to *rejoin* the hard particles becomes larger than the corresponding emission rate, and the soft particle number density in fact *decreases* due to inelastic scatterings. This is the case in the Region B below $p \sim \alpha^{\frac{59a}{268}} Q_s$. The total rate for soft particles rejoining to hard particles is (see Eq. (2.54) of KM1)

$$\Gamma_{\text{rejoin}}(p) \sim \frac{1}{n(p)} \int_{k \sim Q_s} d^3k \Gamma_{\text{split}}(p) \frac{p}{k} f(k) f(p) \sim \frac{n_{\text{hard}}}{Q_s} \frac{\Gamma_{\text{split}}(p)}{p^2} \sim \alpha^{\frac{8+13a}{8}} Q_s (Q_s/p)^{\frac{5}{2}}, \quad (3.17)$$

so that the modes at scales below p_{\max} , with $\Gamma_{\text{rejoin}}(p_{\max})t \lesssim 1$ or

$$p_{\max} \sim \alpha^{\frac{a}{4}} Q_s \quad (3.18)$$

have had time to change their occupancies by an order 1 amount and adjust to the form of Eq. (3.16). Below p_{\max} the occupancies then read

$$f(p) \sim \alpha^{-1+\frac{7}{8}a} (Q_s/p). \quad (3.19)$$

This is the region C of Figure 5.

B. Middle stage: $8/7 < a < 12/5$

1. $a > 8/7$ New particles, the scale k_{old}

For $a > 8/7$, the Bose stimulation for the particle production is lost. As a result, the particle production rate decreases more slowly and particles produced at later times may start to dominate the particle number density. The number of soft particles created at the time scale a is now (remove α^{-c} from Eq. (3.6))

$$n_{\text{daughter}}(p, a) \sim n_{\text{hard}} \alpha t_{\text{form}}^{-1} t \sim \alpha^{\frac{5a}{8}} Q_s^3 (Q_s/p)^{\frac{1}{2}}. \quad (3.20)$$

For $k > k_{\text{iso}}$ this becomes dominant over the redshifted particles for $k < k_{\text{old}}$ given by (compare Eq. (3.20) with Eq. (3.9))

$$k_{\text{old}} \sim \alpha^{\frac{3}{8} - \frac{9a}{64}} Q_s. \quad (3.21)$$

For $k < k_{\text{iso}}$ the new particles become more numerous for $k > k_{\text{old}}$ with (Eq. (3.20) and Eq. (3.13))

$$k_{\text{old}} \sim \alpha^{-\frac{7}{16} + \frac{73a}{128}} Q_s. \quad (3.22)$$

These are the regions D and E in Figure 5, respectively. Region B ends at $a = \frac{56}{41}$.

2. $a > 16/11$: *Soft joining, the scale p_{max}*

We defined the scale p_{max} as the one below which $f(p < p_{\text{max}}) \propto 1/p$. At early times we saw p_{max} is set by the rate of emission/absorption off hard $p \sim Q_s$ excitations. At later times, merging processes between $p \sim p_{\text{max}}$ excitations can become faster and come to control this scale. The rate for soft joining (in Region E, just above p_{max}) is

$$\Gamma_{\text{merge}}(p) \sim \alpha t_{\text{form}}^{-1}(p, \theta \sim 1)[1+f(p)] \sim \alpha^{1 + \frac{21a}{16}} (Q_s/p)^4 Q_s, \quad (3.23)$$

and $\Gamma_{\text{merge}}(p_{\text{max}})t > 1$, using p_{max} from Eq. (3.18), after time $a = 16/11$. After this, the evolution of p_{max} is controlled by soft merging;

$$\Gamma_{\text{merge}}(p_{\text{max}})t \sim 1 \quad \Rightarrow \quad p_{\text{max}} \sim \alpha^{\frac{1}{4} + \frac{5a}{64}} Q_s. \quad (3.24)$$

Modes with $p \lesssim p_{\text{max}}$ effectively thermalize with each other. The energy density is dominated by $p \sim p_{\text{max}}$ modes, so the occupancy is determined by the energy density of particles residing at the scale p_{max} . Hence, for $p < p_{\text{max}}$,

$$f(p) \sim \frac{f(p_{\text{max}})p_{\text{max}}}{p} \sim \alpha^{-\frac{5}{8} + \frac{55a}{128}} (Q_s/p). \quad (3.25)$$

This is Region G in Figure 5.

3. $a > 96/55$: *New plasma instabilities, the scale $k_{\text{new-inst}}$*

The distribution of daughter particles is anisotropic; therefore the daughter particles also give rise to plasma instabilities. As discussed in KM1, the strongest instabilities are driven by daughters at the scale k_{iso} , where the angular distribution is order-1 anisotropic. The resulting plasma instabilities give rise to momentum diffusion

$$\hat{q}_{\text{new-inst}} \sim m^3(k_{\text{iso}}) \sim \alpha^{\frac{3}{2}} f^{\frac{3}{2}}(k_{\text{iso}}) k_{\text{iso}}^3, \quad (3.26)$$

which is comparable in all angular directions θ (see Eq. (4.21-4.22) of KM1). By comparing Eq. (3.1) to Eq. (3.26), using Eq. (3.4) and Eq. (3.20), we find that $\hat{q}_{\text{new-inst}} = \hat{q}_{\text{inst}}$ at large angles $\theta \sim 1$ at $a = 96/55$. After this, the evolution of the scale k_{iso} is driven by the instabilities caused by the scale k_{iso} itself. The scale k_{iso} can be found by self-consistently solving

$$k_{\text{iso}}^2 \sim \hat{q}_{\text{new-inst}} t \quad \text{and} \quad \hat{q}_{\text{new-inst}} \sim \alpha^{\frac{3}{2}} f^{\frac{3}{2}}(k_{\text{iso}}) k_{\text{iso}}^3 \quad \text{with} \quad f(k_{\text{iso}}) \sim \alpha^{\frac{5a}{8}} Q_s^{\frac{7}{2}} k_{\text{iso}}^{-\frac{7}{2}} \quad (3.27)$$

resulting in

$$k_{\text{iso}} \sim \alpha^{\frac{24-a}{68}} Q_s, \quad \hat{q}_{\text{new-inst}} \sim \alpha^{\frac{24+33a}{34}} Q_s^3, \quad f(k_{\text{iso}}) \sim \alpha^{\frac{-42+23a}{34}}. \quad (3.28)$$

When $\hat{q}_{\text{new-inst}}$ dominates, particles at scales above k_{iso} will have an angular range $\theta \sim \alpha^{\frac{24-a}{68}} (Q_s/p)$. The range of angles where $\hat{q}_{\text{new-inst}} > \hat{q}_{\text{inst}}$ is $\theta > \alpha^{\frac{55a-96}{136}}$. Using Eq. (3.3), we see that excitations experience $\hat{q}_{\text{new-inst}}$ provided $p < k_{\text{new-inst}} \sim \alpha^{\frac{144-57a}{136}} Q_s$. This is the region H in Figure 5.

The new \hat{q} changes the rate of the soft merging and therefore the functional form of p_{max} as well as $f(p < p_{\text{max}})$. Repeating the analysis of Subsection III B 2 with $\hat{q} \sim \hat{q}_{\text{new-inst}}$ gives

$$p_{\text{max}} \sim \alpha^{\frac{184+15a}{544}} Q_s \quad \text{and} \quad f(p) \sim \alpha^{\frac{605a-920}{1088}} (Q_s/p). \quad (3.29)$$

This is the region I in Figure 5.

4. $a > 56/25$: Thermalization of the soft sector and the scale k_{split}

At the time $a = 56/25$, $f(p_{\text{max}})$ drops to ~ 1 and the cascade of the infrared modes by joining processes, which started at the time scale $a = 16/11$, is complete. The soft sector now forms a nearly-thermal bath with a temperature $T \sim p_{\text{max}}$. Subsequently, the dominant inelastic process changes from joining to splitting, and those particles with $p > T$ that have had time to undergo a democratic splitting (i.e., emit a daughter with a momentum comparable to emitter's momentum) in less than the system age cascade down in energy by multiple splittings, and lose their energy to the thermal bath. The modes which have had time to undergo a democratic splitting are those for which $p < k_{\text{split}}$, with

$$\Gamma_{\text{split}}(k_{\text{split}})t \sim \alpha t_{\text{form}}^{-1} t \sim 1 \quad \Rightarrow \quad k_{\text{split}} \sim \alpha^2 \hat{q}_{\text{new-inst}} t^2 \sim \alpha^{\frac{92-35a}{34}} Q_s. \quad (3.30)$$

The temperature of the bath is set by the highest momentum modes falling onto it, so that the temperature becomes

$$T \sim \varepsilon^{\frac{1}{4}} \sim (f(k_{\text{split}})k_{\text{split}}^4)^{\frac{1}{4}} \sim \alpha^{\frac{184+15a}{544}} Q_s. \quad (3.31)$$

This explains Region J in Figure 5.

Most of the excitations below k_{iso} but above T have had time to split and release their energy to the thermal bath. However, a small portion of the particles, the ones created in the last time scale $t_{\text{residence}} \sim \Gamma_{\text{split}}^{-1}(p) \sim (p/k_{\text{split}})^{1/2} t$, are still around and have not yet undergone the cascade to lower scales. The flux of energy from the scale k_{split} moving through scales to the scale T is

$$\frac{d\varepsilon}{dt} \sim \varepsilon(k_{\text{split}})/t \sim f(k_{\text{split}})k_{\text{split}}^4/t, \quad (3.32)$$

so that the energy density carried by particles created in the last $t_{\text{residence}}$ time scale at the momentum scale p is

$$\varepsilon(p) \sim t_{\text{residence}} \frac{d\varepsilon}{dt}, \quad (3.33)$$

so that $f(p)$ and $n(p)$ for $k_{\text{iso}} > p > T$ are

$$f(p) \sim \varepsilon(p)/p^4 \sim f(k_{\text{split}})(k_{\text{split}}/p)^{\frac{7}{2}} \sim \alpha^{\frac{5a}{8}} (Q_s/p)^{\frac{7}{2}}, \quad n(p) \sim \alpha^{\frac{5a}{8}} (Q_s/p)^{\frac{1}{2}} Q_s^3 \quad (3.34)$$

which is a continuation of Region E.

5. $a > 160/69$: *Instabilities from the nearly thermal bath*

At time $a = 160/69$ the scale k_{split} crosses the scale k_{iso} . This reduces the number of excitations at the scale k_{iso} , which ceases to dominate as a source of plasma instabilities. However, the thermal bath is incompletely isotropic, so it also gives rise to plasma instabilities, with associated momentum broadening parameter $\hat{q}_{T\text{inst}}$. Beyond $a = 160/69$, $\hat{q}_{T\text{inst}}$ dominates for $\theta \sim 1$.

Two mechanisms keep the soft nearly-thermal bath incompletely isotropic. First, Bjorken expansion continually “stretches” the thermal bath. Secondly, because $\hat{q}_{\text{new-inst}}$ is order-1 anisotropic, the radiated daughters which arrive at the scale T do so with an $\mathcal{O}(1)$ small- θ bias. Both mechanisms return a level of anisotropy for the bath of

$$\epsilon_{\text{bath}} \sim \frac{T^2}{\hat{q}_{T\text{inst}} t}, \quad (3.35)$$

which is the ratio of a typical p_{\perp}^2 in the bath to the change in p_{\perp}^2 during the system’s age.

Using Eq. (3.16) of KM1, we find

$$\hat{q}_{T\text{inst}} \sim \epsilon_{\text{bath}}^{\frac{3}{2}} m(T)^3 \sim \epsilon_{\text{bath}}^{\frac{3}{2}} \alpha^{\frac{3}{2}} T^3. \quad (3.36)$$

Substituting $\hat{q}_{T\text{inst}}$ into Eq. (3.35), we find

$$\epsilon_{\text{bath}} \sim \alpha^{-\frac{3}{5}} (tT)^{-\frac{2}{5}}, \quad \hat{q}_{T\text{inst}} \sim \alpha^{\frac{3}{5}} T^{\frac{12}{5}} t^{-\frac{3}{5}}. \quad (3.37)$$

The temperature is still determined by the k_{split} scale, $T \sim (f(k_{\text{split}}))^{1/4} k_{\text{split}}$, and the splitting scale is given by $k_{\text{split}} \sim \alpha^2 \hat{q}_{T\text{inst}} t^2$. Solving self-consistently for ϵ , $\hat{q}_{T\text{inst}}$, k_{split} , and T gives

$$T \sim \alpha^{\frac{13}{28} - \frac{3a}{112}} Q_s, \quad \hat{q}_{T\text{inst}} \sim \alpha^{\frac{12}{7} + \frac{15a}{28}} Q_s^3, \quad k_{\text{split}} \sim \alpha^{\frac{26}{7} - \frac{41a}{28}} Q_s, \quad \epsilon_{\text{bath}} \sim \alpha^{\frac{-44+23a}{56}}. \quad (3.38)$$

This explains Region K in Figure 5.

The new dominant \hat{q} changes the rate of angular broadening and hence also the scale $k_{\text{new-inst}}$. The momentum range where $\hat{q}_{\text{new-inst}}$ dominates, and the angular range of excitations, are

$$\hat{q}_{T\text{inst}} > \hat{q}_{\text{inst}} \text{ if } p < k_{\text{new-inst}} \sim \alpha^{\frac{36-15a}{14}} Q_s \quad \text{where} \quad \theta \sim \alpha^{\frac{48-13a}{56}} Q_s/p. \quad (3.39)$$

This explains Regions L and M, above and below k_{old} , respectively.

Below k_{split} but above T the cascading particles start their fall in a small angle range at the scale k_{split} and as they cascade down in energy, their angular range broadens. The cascading particles stay at the momentum scale p for the time $t_{\text{residence}} \sim (p/k_{\text{split}})^{1/2} t$, and during this time their angular range grows to

$$p^2 \theta^2 \sim \hat{q}_{T\text{inst}} t_{\text{residence}} \quad \Rightarrow \quad \theta \sim \alpha^{\frac{-8+15a}{112}} (Q_s/p)^{\frac{3}{4}} \quad (3.40)$$

with $\theta \sim 1$ for $p \lesssim k_{\text{iso}} \sim \alpha^{\frac{-8+15a}{84}} Q_s$. The estimate for the particle number density from Eq. (3.34) still holds so that the occupation number below k_{split} is $f(p) \sim \alpha^{\frac{8+55a}{112}} (Q_s/p)^{\frac{11}{4}}$. This is Region N in Figure 5.⁵

⁵ A quick calculation of \hat{q} due to instabilities associated with the scale k_{iso} returns $\hat{q}_{\text{new-inst}} \sim \alpha^{\frac{48+15a}{28}} Q_s^3 \sim \hat{q}_{T\text{inst}}$. All scales from k_{iso} down to T actually have comparable roles in setting \hat{q} ; but this does not change parametric estimates.

C. Late stages: $12/5 < a < 5/2$

At $a = 12/5$ we find $\hat{q}_{\text{inst}} \sim \hat{q}_{T_{\text{inst}}}$. Beyond this scale, the new plasma instabilities from the incompletely isotropic thermal bath dominate momentum broadening at *all* scales, i.e., this is the first moment when the soft sector starts to influence the dynamics of the hard particles. This is the point $d = 3/10$, $c = -11/10$ in Figure 2, where attractor 1 enters the region marked “Soft Particle Bath Forms.” As a result, the anisotropy of the hard modes departs from $d = a/8$ to become more isotropic, and the rate of radiation of daughters increases, since it is now controlled by the larger $\hat{q}_{T_{\text{inst}}}$.

The splitting scale is now given by $k_{\text{split}} \sim \alpha^2 \hat{q}_{T_{\text{inst}}} t^2$. Since there is only a single \hat{q} , k_{split} is the scale where there is of order 1 daughter per hard particle. So

$$T^4 \sim n_{\text{hard}} k_{\text{split}} \sim \alpha^{1-a} \hat{q}_{T_{\text{inst}}} Q_s \quad (3.41)$$

while Eq. (3.37) still holds. Solving self-consistently, we find

$$\hat{q}_{T_{\text{inst}}} \sim \alpha^3 Q_s^3, \quad T \sim \alpha^{1-\frac{a}{4}} Q_s, \quad k_{\text{split}} \sim \alpha^{5-2a} Q_s, \quad \epsilon_{\text{bath}} \sim \alpha^{\frac{a-2}{2}}. \quad (3.42)$$

This is Region O in Figure 5.

The new \hat{q} broadens the angular distribution more effectively, and for $p > k_{\text{split}}$ we find $\theta(p) \sim \alpha^{\frac{3-a}{2}} Q_s/p$. In particular, the angular range of the primary hard excitations is $\delta \sim \alpha^{\frac{3-a}{2}}$, which grows with time for the first time since $a \simeq 0$. However, the hard excitations remain anisotropic to the bitter end.

Repeating the calculation of the behavior of particles within the cascade, we get the results for regions P, Q, R, and S in Figure 5.

The thermal bath continues to draw energy from the hard excitations until k_{split} reaches Q_s and the hard excitations, which dominate the system’s energy, themselves split and join the thermal bath. This occurs at $a = 5/2$. At this stage the temperature is $T \sim \alpha^{\frac{3}{8}} Q_s$, and the residual anisotropy of the nearly-thermal bath is $\epsilon \sim \alpha^{\frac{1}{4}}$. This is still larger than the value $\epsilon \sim \alpha^{\frac{1}{3}}$ where a thermal bath becomes dominated by scattering rather than plasma instabilities.

A shortcut calculation which leads to the correct final equilibration time is the following. The energy density scales with time as $\epsilon \sim \alpha^{a-1} Q_s^4$, so the would-be equilibration temperature is $T(a) \sim \alpha^{\frac{a-1}{4}} Q_s$. According to KM1 [17], the equilibration time for an anisotropic system with $T < Q_s$ is

$$t_{\text{eq}} \sim \alpha^{\frac{-13}{7}} Q_s^{\frac{5}{7}} T^{\frac{-12}{7}}. \quad (3.43)$$

(This result was derived by asking how long it takes a thermal bath at temperature T to cause hard splitting in excitations of momentum Q_s , given that the thermal bath will be somewhat anisotropic and the dynamics are dominated by plasma instabilities; see KM1 [17].) Equating t_{eq} with the age of the system $t \sim \alpha^{-a} Q_s^{-1}$ and inserting our expression for T , we find $a = 5/2$ or $t_{\text{eq}} \sim \alpha^{\frac{-5}{2}} Q_s^{-1}$.

D. Aftermath: $a > 5/2$

After $a = 5/2$ the $p \sim Q_s$ initial excitations are gone, leaving behind a nearly thermal bath. The system is again characterized by a single scale, the temperature T , and hence

the system can again be described using Figure 2. At the time $a = 5/2$, $d = -1/4$ and $c = 0$; subsequent evolution makes the distribution more isotropic, and the solution will move down along the d -axis.

The system is now nearly isotropic, and therefore the energy density begins to scale with time as $\epsilon \propto t^{-4/3}$ rather than as t^{-1} . Using the value of the energy density at $a = 5/2$, we find

$$T \sim \alpha^{\frac{a}{3} - \frac{11}{24}} Q_s. \quad (3.44)$$

Initially \hat{q} remains dominated by plasma instabilities from the residual anisotropy of the thermal bath giving rise to ‘‘anomalous viscosity’’. We still find Eq. (3.37) to hold; substituting the known T value,

$$\hat{q} \sim \alpha^{\frac{7a}{5} - \frac{1}{2}} Q_s^3, \quad \epsilon \sim \alpha^{\frac{4a}{15} - \frac{5}{12}}. \quad (3.45)$$

This drops below the value $\epsilon \sim \alpha^{1/3}$, entering the regime where ordinary scattering dominates, at $a = 45/16$. Beyond this time scale, the system behaves like an ordinary thermal bath expanding with a viscosity given by the normal (non-anomalous) viscous law; $\hat{q} \sim \alpha^2 T^3 \sim \alpha^{a + \frac{5}{8}} Q_s^3$ and the residual anisotropy is $\epsilon \sim \alpha^{\frac{2a}{3} - \frac{37}{24}}$.

In comparison, attractor 2 reaches the d -axis at the time $a = 135/56$, so that the system becomes nearly thermal slightly earlier than in the case of the first attractor. As a consequence of being nearly isotropic from the beginning, the temperature is now only

$$T_{\text{att2}} \sim \alpha^{\frac{a}{3} - \frac{1}{4}} Q_s \quad (3.46)$$

resulting in

$$\hat{q}_{\text{att2}} \sim \alpha^{\frac{7a}{5}} Q_s^3, \quad \epsilon_{\text{att2}} \sim \alpha^{\frac{4a}{15} - \frac{1}{2}}. \quad (3.47)$$

In the case of attractor 2, scattering comes to dominate at the time $a = 25/8$, after which $\hat{q}_{\text{att2}} \sim \alpha^{a + \frac{5}{4}} Q_s^3$ and $\epsilon_{\text{att2}} \sim \alpha^{\frac{2a}{3} - \frac{7}{4}}$.

In both cases, the behavior after scattering comes to dominate continues, in principle, indefinitely. At exponentially late times, $a \simeq 3\alpha^{-1}/\beta_0 \ln(\alpha^{-1})$, the temperature scale reaches Λ_{QCD} and hadronization occurs.

IV. DISCUSSION

We have presented a complete parametric description of thermalization after a heavy ion collision in the theoretically clean, in-principle limit of arbitrarily large and high-energy ions, such that the scale Q_s (which dominates particle production from the original collision) is taken so large that $\alpha_s(Q_s) \ll 1$. Our most significant finding is that thermalization does eventually occur. Plasma instabilities dominate the dynamics at all times until well after the system becomes nearly isotropic and thermal. Initially, they cause the highly anisotropic starting configuration to become order-1 isotropic. But Bjorken expansion, and falling typical occupancies, allow the system to again become anisotropic – though the level of anisotropy only grows as $t^{\frac{1}{8}}$.

The process of thermalization is dominated by

1. the generation of plasma instabilities due to the anisotropy of the typical $p \sim Q_s$ excitations;
2. the radiation of daughter excitations, which eventually form a nearly-thermal bath;

3. the plasma instabilities generated by the residual anisotropy of these daughter excitations, which are responsible for finally breaking up the $p \sim Q_s$ excitations and thermalizing the system at a time scale $t \sim \alpha^{-\frac{5}{2}} Q_s^{-1}$.

After near-thermalization the system remains dominated by plasma instabilities of a nearly-thermal bath (anomalous viscosity) until the time scale $t \sim \alpha^{-\frac{45}{16}} Q_s^{-1}$, after which elastic scattering becomes the most important physical process and the plasma is well described by standard kinetic theory.

Since there is an extended period of expansion in which the equation of state is $\varepsilon \propto t^{-1}$ rather than $\varepsilon \propto t^{-\frac{4}{3}}$ as for a thermal system, there is significant entropy generation. Most of the entropy of the final system is generated around $t \sim \alpha^{-\frac{5}{2}} Q_s^{-1}$, when the initial hard excitations fragment and join the thermal bath. This entropy generation could have phenomenological consequences in connecting the Colored Glass initial conditions to final state multiplicities, see [27].

It is not clear to us how high Q_s would actually need to be for the parametric estimates of this paper really to make sense. However we feel that this work does resolve the long-standing puzzle of what happens in a heavy ion collision in what should be the most theoretically clean limit – that of extremely large saturation scale.

It would be nice to replace this *parametric* estimate with a *numerical* estimate, by computing the “constant” in $t_{\text{therm}} = (\#)\alpha^{\frac{-5}{2}} Q_s^{-1}$. The good news is that this only requires one to study the final stage of thermalization, $12/5 < a < 5/2$ (since all other stages take parametrically less time). To study the relevant physics in this stage, we would need to determine the relationship between anisotropy ϵ and momentum diffusion \hat{q} for a nearly thermal bath, and we would need to compute the exact rate of fragmentation for a hard excitation experiencing a given value of \hat{q} . The former could be done by studying the plasma instabilities of a weakly anisotropic system. This should be doable using existing methods which combine classical field dynamics with anisotropic hard loops. The latter is also straightforward.

Acknowledgements

This work was supported in part by the Natural Sciences and Engineering Research Council of Canada and the Institute of Particle Physics (Canada).

-
- [1] K. Adcox *et al.* [PHENIX Collaboration], Nucl. Phys. A **757** (2005) 184; B. B. Back *et al.* [PHOBOS Collaboration], Nucl. Phys. A **757** (2005) 28; I. Arsene *et al.* [BRAHMS Collaboration], Nucl. Phys. A **757** (2005) 1; J. Adams *et al.* [STAR Collaboration], Nucl. Phys. A **757** (2005) 102.
 - [2] K. Aamodt *et al.* [The ALICE Collaboration], Phys. Rev. Lett. **105**, 252302 (2010). [arXiv:1011.3914 [nucl-ex]].
 - [3] D. Teaney, J. Lauret and E. V. Shuryak, Phys. Rev. Lett. **86** (2001) 4783; P. Huovinen, P. F. Kolb, U. W. Heinz, P. V. Ruuskanen and S. A. Voloshin, Phys. Lett. B **503** (2001) 58; P. F. Kolb, U. W. Heinz, P. Huovinen, K. J. Eskola and K. Tuominen, Nucl. Phys. A **696** (2001) 197; T. Hirano and K. Tsuda, Phys. Rev. C **66** (2002) 054905; P. F. Kolb and R. Rapp, Phys. Rev. C **67** (2003) 044903.

- [4] P. Romatschke and U. Romatschke, Phys. Rev. Lett. **99**, 172301 (2007); M. Luzum and P. Romatschke, Phys. Rev. C **78**, 034915 (2008) [Erratum-ibid. C **79**, 039903 (2009)]; K. Dusling and D. Teaney, Phys. Rev. C **77**, 034905 (2008); H. Song and U. W. Heinz, Phys. Rev. C **77**, 064901 (2008).
- [5] For reviews see for instance, E. Iancu, R. Venugopalan, In *Hwa, R.C. (ed.) et al.: Quark gluon plasma* 249-3363. [hep-ph/0303204]; F. Gelis, E. Iancu, J. Jalilian-Marian and R. Venugopalan, Ann. Rev. Nucl. Part. Sci. **60**, 463 (2010) [arXiv:1002.0333 [hep-ph]].
- [6] L. D. McLerran, R. Venugopalan, Phys. Rev. **D49**, 2233-2241 (1994). [arXiv:hep-ph/9309289 [hep-ph]]; Phys. Rev. **D49**, 3352-3355 (1994). [hep-ph/9311205]. J. Jalilian-Marian, A. Kovner, L. D. McLerran, H. Weigert, Phys. Rev. **D55**, 5414-5428 (1997). [hep-ph/9606337].
- [7] A. Kovner, L. D. McLerran, H. Weigert, Phys. Rev. **D52**, 6231-6237 (1995). [hep-ph/9502289]. A. Krasnitz, R. Venugopalan, Phys. Rev. Lett. **84**, 4309-4312 (2000). [hep-ph/9909203]. T. Lappi and L. McLerran, Nucl. Phys. A **772**, 200 (2006) [arXiv:hep-ph/0602189].
- [8] J. Jalilian-Marian, A. Kovner, A. Leonidov, H. Weigert, Phys. Rev. **D59**, 014014 (1999). [hep-ph/9706377]; Y. V. Kovchegov, Phys. Rev. **D60**, 034008 (1999). [hep-ph/9901281]; E. Iancu, A. Leonidov, L. D. McLerran, Nucl. Phys. **A692**, 583-645 (2001). [hep-ph/0011241].
- [9] R. Baier, A. H. Mueller, D. Schiff and D. T. Son, Phys. Lett. B **502**, 51 (2001) [hep-ph/0009237].
- [10] P. B. Arnold, J. Lenaghan and G. D. Moore, JHEP **0308**, 002 (2003) [hep-ph/0307325].
- [11] S. Mrówczyński, Phys. Lett. B **214**, 587 (1988). Phys. Lett. B **314**, 118 (1993). S. Mrówczyński and M. H. Thoma, Phys. Rev. D **62**, 036011 (2000) [hep-ph/0001164].
- [12] P. Romatschke and M. Strickland, Phys. Rev. D **68**, 036004 (2003) [hep-ph/0304092]; Phys. Rev. D **68**, 036004 (2003) [hep-ph/0304092].
- [13] D. Bödeker, JHEP **0510**, 092 (2005) [arXiv:hep-ph/0508223].
- [14] P. B. Arnold and G. D. Moore, Phys. Rev. D **76**, 045009 (2007) [0706.0490 [hep-ph]].
- [15] P. Romatschke, R. Venugopalan, Phys. Rev. Lett. **96**, 062302 (2006). [hep-ph/0510121]; Phys. Rev. **D74**, 045011 (2006). [hep-ph/0605045].
- [16] P. Romatschke, A. Rebhan, Phys. Rev. Lett. **97**, 252301 (2006). [hep-ph/0605064]. A. Rebhan, M. Strickland, M. Attems, Phys. Rev. **D78**, 045023 (2008). [arXiv:0802.1714 [hep-ph]]. A. Rebhan, D. Steineder, Phys. Rev. **D81**, 085044 (2010). [arXiv:0912.5383 [hep-ph]].
- [17] A. Kurkela, G. D. Moore, arXiv:1107.5050 [hep-ph].
- [18] J. -P. Blaizot, F. Gelis, J. Liao, L. McLerran, R. Venugopalan, arXiv:1107.5296 [hep-ph].
- [19] M. Asakawa, S. A. Bass and B. Muller, Phys. Rev. Lett. **96**, 252301 (2006) [hep-ph/0603092]; Prog. Theor. Phys. **116**, 725 (2007) [hep-ph/0608270].
- [20] P. B. Arnold, J. Lenaghan, Phys. Rev. **D70**, 114007 (2004). [hep-ph/0408052].
- [21] E. S. Weibel, Phys. Rev. Lett. **2**, 83 (1959).
- [22] N. K. Nielsen and P. Olesen, Nucl. Phys. B **144**, 376 (1978).
- [23] P. B. Arnold, C. Dogan and G. D. Moore, Phys. Rev. D **74**, 085021 (2006) [arXiv:hep-ph/0608012].
- [24] D. Polarski and A. A. Starobinsky, Class. Quant. Grav. **13**, 377 (1996) [arXiv:gr-qc/9504030]; S. Y. Khlebnikov and I. I. Tkachev, Phys. Rev. Lett. **77**, 219 (1996) [arXiv:hep-ph/9603378].
- [25] A. Rebhan, P. Romatschke, M. Strickland, Phys. Rev. Lett. **94**, 102303 (2005). [hep-ph/0412016].
- [26] D. Bödeker, K. Rummukainen, JHEP **0707**, 022 (2007). [arXiv:0705.0180 [hep-ph]].
- [27] R. Baier, A. H. Mueller, D. Schiff, D. T. Son, Phys. Lett. **B539**, 46-52 (2002). [hep-ph/0204211]; [arXiv:1103.1259 [nucl-th]].